Neuron, Vol. 42, 253–268, April 22, 2004, Copyright ©2004 by Cell Press

Synchronized Oscillations at α and θ Frequencies in the Lateral Geniculate Nucleus

Stuart W. Hughes,[1,*] Magor Lörincz,[2] David W. Cope,[1] Kate L. Blethyn,[1] Katalin A. Kékesi,[2] H. Rheinallt Parri,[2] Gábor Juhász,[2] and Vincenzo Crunelli[1]
[1]School of Biosciences
Cardiff University
Museum Avenue
Cardiff CF10 3US
United Kingdom
[2]Research Group of Neurobiology
Hungarian Academy of Sciences
Pázmány P. st. 1C 1117
Budapest
Hungary

Summary

In relaxed wakefulness, the EEG exhibits robust rhythms in the α band (8–13 Hz), which decelerate to θ (~2–7 Hz) frequencies during early sleep. In animal models, these rhythms occur coherently with synchronized activity in the thalamus. However, the mechanisms of this thalamic activity are unknown. Here we show that, in slices of the lateral geniculate nucleus maintained in vitro, activation of the metabotropic glutamate receptor (mGluR) mGluR1a induces synchronized oscillations at α and θ frequencies that share similarities with thalamic α and θ rhythms recorded in vivo. These in vitro oscillations are driven by an unusual form of burst firing that is present in a subset of thalamocortical neurons and are synchronized by gap junctions. We propose that mGluR1a-induced oscillations are a potential mechanism whereby the thalamus promotes EEG α and θ rhythms in the intact brain.

Introduction

In relaxed wakefulness, the human electroencephalogram (EEG) is dominated by rhythms in the α (8–13 Hz) frequency band (Niedermeyer, 1993a). The most pronounced of these is the posterior α rhythm, which is present over the occipital cortex and is maximal when the eyes are closed (Berger, 1933). This rhythm is thought to be influenced by a thalamic "pacemaker" (Lopes da Silva et al., 1973, 1980; Rougeul-Buser and Buser, 1997) because its equivalent in dogs and cats is accompanied by simultaneous and coherent activity in the lateral geniculate nucleus (LGN) (Lopes da Silva et al., 1973; Chatila et al., 1993). Furthermore, these LGN α rhythms are sometimes present even when cortical α rhythms are not (Lopes da Silva et al., 1973), which suggests that they can be generated locally in the thalamus. A similar relationship exists between the somatosensory cortex and thalamus for the cat equivalent of the human μ rhythm (Bouyer et al., 1983), the somatosensory analog of the posterior α rhythm, and for low-frequency rhythms that are associated with relaxed wakefulness in rats (Buzsáki, 1991). Moreover, in both species, these somatosensory rhythms occur synchronously with rhythmic bursting in thalamic neurons (Bouyer et al., 1982; Buzsáki, 1991). Support for a thalamic involvement in α rhythm generation also derives from numerous human studies using positron emission tomography (PET) and functional magnetic resonance imaging (fMRI), which show a correlation between EEG α band power and thalamic metabolic activity (Larson et al., 1998, Lindgren et al., 1999; Danos et al., 2001; Goldman et al., 2002).

During drowsiness, a scenario which is considered to be related to disfacilitation at the thalamic level (Steriade et al., 1993), human α rhythms are briefly replaced by slower θ activity at ~2–7 Hz, prior to the onset of spindle (7–14 Hz) and slow (<1 Hz) waves (Niedermeyer, 1993b). Interestingly, rhythmic activity at a similar frequency (~3–5 Hz) has been observed in the LGN of cats during drowsiness and sleep (Kanamori, 1993) and, as with LGN α rhythms, can occur either in isolation or coherently with activity in the visual cortex, suggesting that it can also be generated intrinsically in the thalamus. Note that this type of θ activity is distinct and unrelated to that occurring in the hippocampus of rats during exploratory behavior and REM sleep (see Buzsáki, 2002).

In this study, we show that, following strong activation of the metabotropic glutamate receptor (mGluR) mGluR1a with either *trans*-ACPD or DHPG, slices of the cat LGN maintained in vitro can generate synchronized oscillations in the α (8–13 Hz) frequency band, whereas more moderate mGluR1a activation slows these oscillations to within the θ (2–7 Hz) range. These oscillations share a common cellular basis, being driven by high-threshold (HT) bursting (Hughes et al., 2002b), which occurs in a subset of TC neurons, and being synchronized by gap junctions. Interestingly, these oscillations share a number of points of similarity with thalamic α and θ rhythms recorded in vivo during relaxed wakefulness and early sleep, respectively. Together with previous studies (Whittington et al., 1995; Beierlein et al., 2000; Deans et al., 2001; Gillies et al., 2002; Long et al., 2004), these results suggest that activation of mGluRs is an important general mechanism for inducing synchronized neuronal activity at a variety of physiologically relevant frequencies and in several distinct brain areas. In particular, we propose that mGluR1a-induced oscillations at α and θ frequencies represent a potential route whereby the thalamus promotes EEG α and θ activity in the intact brain.

Results

Activation of mGluR1a Instates α, θ, and Slow Waves in the LGN Slice

In control conditions, extracellular field recordings from slices of the cat LGN in vitro showed a lack of spontaneous activity (n = 68) (Figure 1A). However, the nonspe-

*Correspondence: hughessw@cardiff.ac.uk

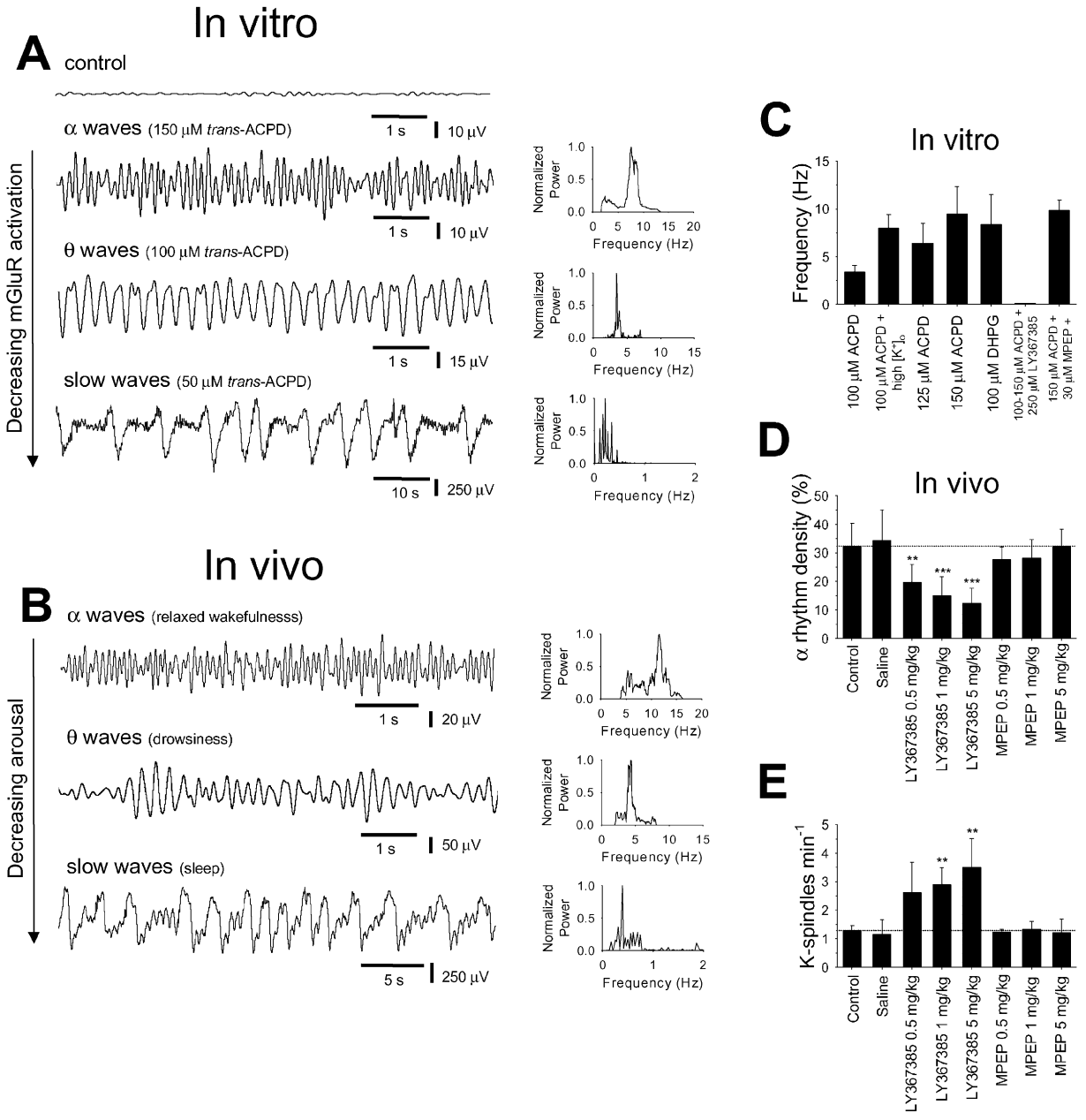

Figure 1. α, θ, and Slow Waves in the LGN In Vitro and In Vivo and Their Dependence on mGluR1a

(A) Extracellular field recording in the LGN slice showing a lack of activity in control conditions (top trace). 150 μM *trans*-ACPD induces a robust oscillation at ~8 Hz with a characteristic sinusoidal appearance and seemingly random waxing and waning nature. This oscillation slows to ~4 Hz when the concentration of *trans*-ACPD is reduced to 100 μM and is replaced by slow waves at <1 Hz when the concentration is further reduced to 50 μM. All data were taken from the same LGN recording site. (B) A similar series of field oscillations is observed in the LGN in vivo as arousal shifts from a state of relaxed wakefulness (α waves), through drowsiness (θ waves), to deep sleep (slow waves). Again, all data were taken from the same LGN recording site. (C) Histograms showing the mean frequency of in vitro α/θ oscillations under various conditions and their dependence on mGluR1a. (D and E) Histogram showing the effect of i.v. injection of mGluR antagonists at various doses on in vivo α rhythm density and frequency of K spindle complexes in LGN field recordings. **$p < 0.001$; ***$p < 0.0001$. Numbers of observations for the data presented in (C)–(E) are given in the text.

cific group I/II mGluR agonist *trans*-ACPD (100–150 μM) (n = 52) induced prominent waxing and waning oscillations at ~2–13 Hz that were extremely robust and could remain unaltered for long recording periods (>3 hr). The mean frequency of oscillations following 150 μM *trans*-ACPD application was 9.5 ± 1.0 Hz (range, 4.3–13.7 Hz; n = 10 slices) or generally within the α range. Oscillations following 100 μM *trans*-ACPD application occurred at 3.4 ± 0.2 Hz (range, 2.8–4.5 Hz; n = 13), corresponding to the θ band (Figures 1A and 1C). Collectively, we termed these oscillations α/θ oscillations. The frequency of α/θ oscillations was modulated by elevating $[K^+]_o$ (100 μM

trans-ACPD + 3.25mM $[K^+]_o$: 3.4 ± 0.2 Hz, n = 13; 100 μM *trans*-ACPD + 5mM $[K^+]_o$: 8.0 ± 0.6 Hz, n = 6; $p < 0.001$), suggesting that oscillation frequency increases with neuronal depolarization (Figure 1C). Reducing the *trans*-ACPD concentration below 100 μM led to the appearance of large-amplitude slow (<1 Hz) waves (peak-to-peak amplitude, 0.7 ± 0.1 mV; frequency, 0.15 ± 0.02 Hz; n = 5 with 50 μM *trans*-ACPD) with a similar appearance to those observed in vivo during deep sleep (Figure 1B) (cf. Amzica and Steriade, 1998). As the *trans*-ACPD concentration was further reduced, these slow waves steadily increased in frequency before being ultimately abolished following a full washout (data not shown).

The effect of *trans*-ACPD in bringing about α/θ oscillations was mediated through mGluR1a since (1) these activities could also be instated by the group I-specific mGluR agonist DHPG (mean frequency of α/θ oscillations at 100 μM, 8.4 ± 0.8 Hz; n = 16) (Figure 1C), and (2) *trans*-ACPD-induced α/θ oscillations were abolished by the mGluR1a-specific antagonist LY367385 (250 μM) (n = 5) (Figure 1C) but unaffected by the mGluR5-specific antagonist MPEP (30 μM) (n = 3) (Figure 1C).

Arousal State-Related Field Oscillations in the LGN In Vivo Are also Modulated by mGluR1a Activation

The field oscillations that occur in the LGN slice as the intensity of mGluR1a activation is reduced are similar to those that occur in the LGN in vivo as arousal decreases from a state of relaxed wakefulness through drowsiness to deep sleep (Figure 1B; see also the Supplemental Data and Supplemental Figure S1 at http://www.neuron.org/cgi/content/full/42/2/253/DC1). To test whether mGluR1a plays a role in modulating these in vivo LGN field oscillations, we investigated the effect of mGluR antagonists in freely moving cats. Injection of the mGluR1a-specific antagonist LY367385 (at 0.5, 1, and 5 mg/kg, i.v.) led to a rapid and significant reduction in the density of LGN α rhythms (see Experimental Procedures) ($p < 0.001$ for 0.5 mg/kg; $p < 0.0001$ for 1 and 5 mg/kg; n = 8 for each dose) (Figure 1D). In contrast, neither saline nor the mGluR5-specific antagonist MPEP (at 0.5, 1, and 5 mg/kg i.v.) had an effect (Figure 1D). In normal conditions, animals often remained in a condition of relaxed wakefulness for several (>5) minutes. However, following LY367385 injection, all cats became sleepy and were unable to maintain a state of relaxed wakefulness for more than 1–2 min. To quantify the sedative effect of LY367385, we measured the mean number of K spindle complexes per minute in the hour preceding and following drug injection. K spindle complexes consist of a K complex followed by a brief burst of spindle waves and are an easily identifiable LGN field component (Supplemental Figure S1C) that represent the earliest manifestation of slow sleep waves in the naturally sleeping cat (Amzica and Steriade, 1998). At all doses tested (0.5, 1, and 5 mg/kg, i.v.), LY367385 caused a substantial increase in the frequency of these events, being statistically significant ($p < 0.001$) at doses of 1 and 5 mg/kg (n = 8 for each dose) (Figure 1E). Injection of MPEP had no effect on the number of K spindle events (0.5, 1, and 5 mg/kg i.v.; n = 8 for each dose) (Figure 1E). All of the effects of LY367385 on LGN field recordings were also clearly reflected in occipital cortical EEG recordings (data not shown). Thus, antagonism of mGluR1a in vivo consistently diminished the amount of LGN α activity in favor of sleep-related field oscillations and correspondingly reduced the level of vigilance.

The Neuronal Activity Occurring in the LGN during α/θ Oscillations In Vitro and α and θ Waves In Vivo Is Similar

To determine the neuronal activity associated with in vitro α/θ oscillations, we obtained simultaneous extracellular field and single-unit recordings from the LGN slice preparation. During α/θ oscillations, 20% (63 of 319) of single units displayed correlated bursts of two to seven spikes (Figure 2A; see also the Supplemental Data and Supplemental Figure S3 at http://www.neuron.org/cgi/content/full/42/2/253/DC1) that displayed two main characteristics. First, they exhibited comparatively large interspike intervals (ISIs) (16.5 ± 0.6 ms; n = 120) that did not vary as the burst progressed (Figures 2A and 2C). Second, the mean number of action potentials in these bursts decreased as the interburst frequency increased such that, at interburst frequencies of 10 Hz or greater, activity consisted only of action potential doublets or occasional single spikes (Figures 2A and 2D). Overall, 97% of α/θ oscillation cycles were accompanied by bursts of spikes in the single-unit recordings that displayed correlated activity. During slow waves, the same cells showed a different type of bursting that was characterised by high-frequency (up to 500 Hz) groups of spikes and increasing ISIs as the burst progressed (Figure 2E and Supplemental Figure S2A). Such bursts are generated by low-threshold Ca^{2+} potentials (LTCPs) (Hughes et al., 2002b) (see Figures 3A and 3B) and identify the cells under investigation as thalamocortical (TC) neurons.

Similar patterns of neuronal activity were observed during physiological α, θ, and slow waves in the LGN of freely moving cats (Figure 2B and Supplemental Figure S2B at http://www.neuron.org/cgi/content/full/42/2/253/DC1). Out of a total of 30 simultaneous unit and local field potential recordings obtained from the LGN, we identified single-unit activity in four recordings (13%) that showed correlated firing with both local α and θ field activity (Figure 2B). The remainder of the units did not exhibit correlations with either α or θ waves. The firing associated with in vivo α and θ waves comprised bursts of two to six spikes that occurred close to the negative peaks of the field oscillation and which displayed comparatively large ISIs (17.6 ± 0.7 ms; n = 105) that remained relatively constant throughout the duration of the burst (Figures 2B and 2C). As with the firing related to in vitro α/θ oscillations, the mean number of action potentials in these bursts decreased as the interburst frequency increased such that, at interburst frequencies of 10 Hz or greater, activity consisted only of action potential doublets or occasional single spikes (Figures 2B and 2D). Overall, 87% of α and θ rhythm cycles were accompanied by bursts of spikes in the unit recordings that exhibited correlated firing. As shown previously (McCarley et al., 1983) and in similarity to in vitro recordings, the same cells showed a distinct type

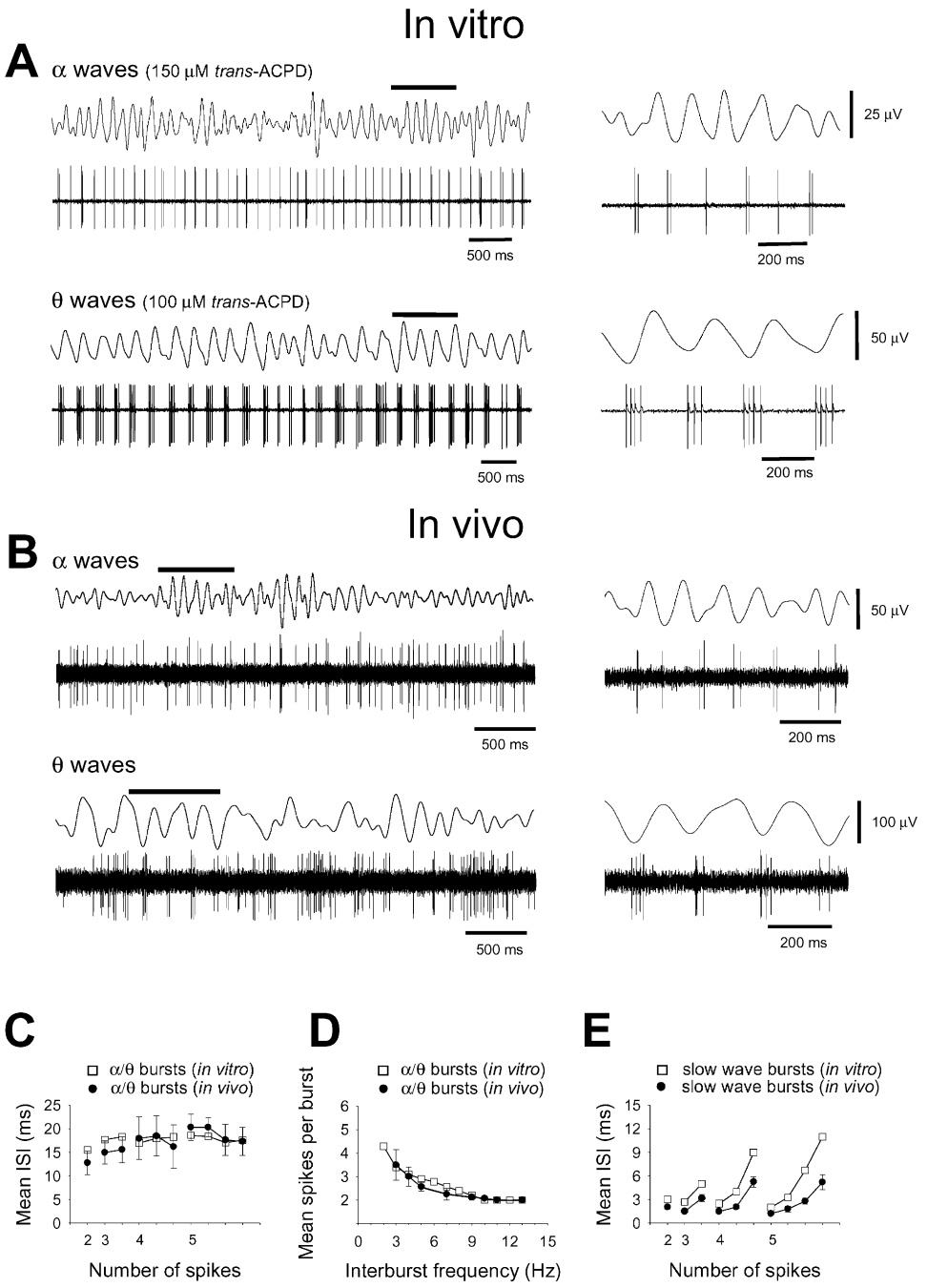

Figure 2. Neuronal Activity in the LGN Related to α/θ Oscillations In Vitro and α and θ Rhythms In Vivo

(A) Simultaneous field and single-unit recording in the LGN in vitro showing correlated activity with both α (upper traces; 150 μM *trans*-ACPD) and θ (lower traces; 100 μM *trans*-ACPD) field oscillations. The sections marked by the continuous bars are enlarged on the right.

(B) Simultaneous field and single-unit recording in the LGN in vivo showing correlated activity with both α (upper traces) and θ (lower traces) field oscillations. The sections marked by the continuous bars are enlarged on the right.

(C) Plots showing the similarity in the averaged ISI patterns for spike bursts correlated to α and θ activity in vivo (●) and in vitro (□).

(D) Plots of interburst frequency versus number of spikes per burst are similar for in vivo (●) and in vitro (□) single-unit recordings during α and θ activity.

(E) Plots showing the similarity in the averaged ISI patterns for spike bursts correlated to slow wave activity in vivo (●) and in vitro (□). Note the contrasting pattern to that occurring during α and θ rhythms (C). Additional information regarding the neuronal activity correlated with in vivo and in vitro slow waves is shown in Supplemental Figure S2 at http://www.neuron.org/cgi/content/full/42/2/253/DC1.

of bursting in relation to local slow waves that was characterised by high-frequency (up to 500 Hz) groups of spikes and increasing ISIs as the burst progressed (Figure 2E and Supplemental Figure S2B).

High-Threshold Bursting in TC Neurons Underlies α/θ Oscillations

To investigate the precise nature of the repetitive burst firing underlying in vitro α/θ oscillations, we performed

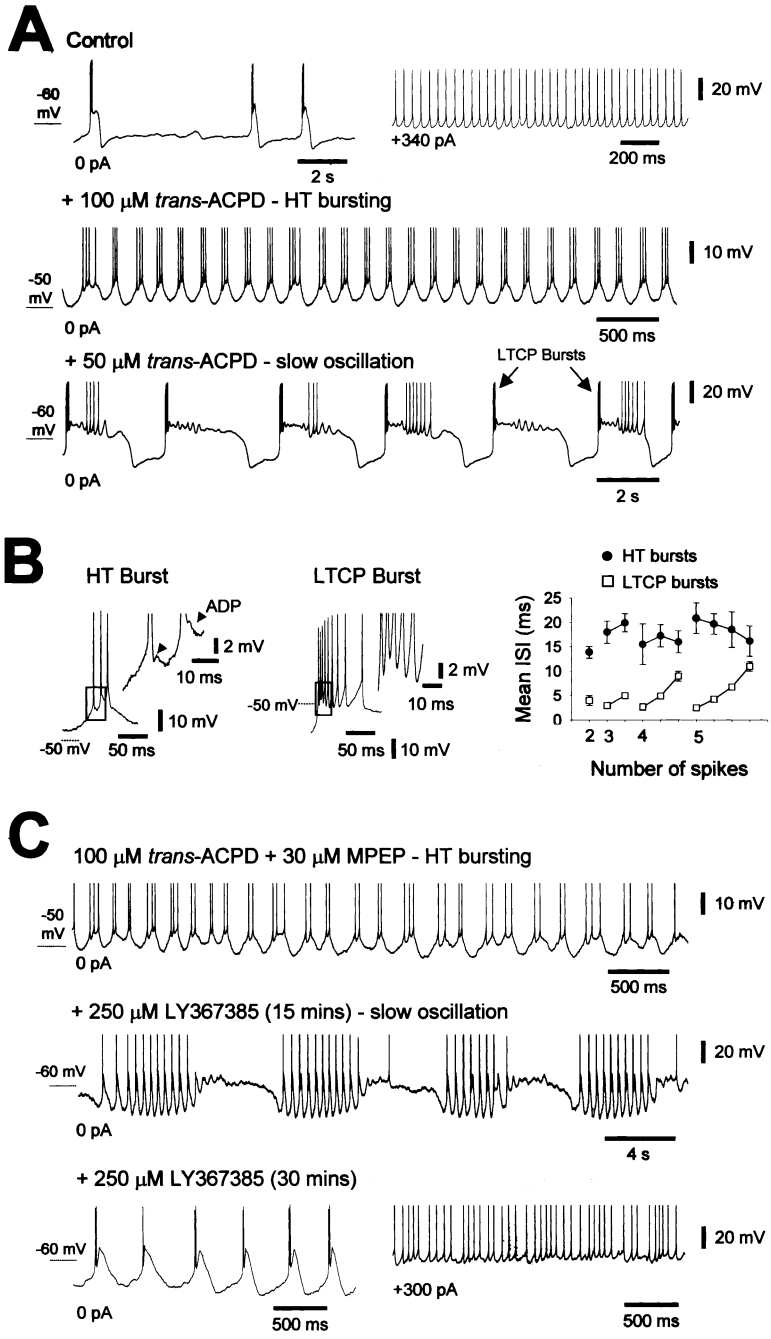

Figure 3. Intracellular Effects of Different Intensities of mGluR Activation on LGN TC Neurons In Vitro

(A) An LGN TC neuron in control conditions exhibiting spontaneous LTCP-mediated bursts in the absence of injected DC current (top left) and tonic firing in response to steady depolarizing current (+340 pA) (top right). 100 μM *trans*-ACPD depolarizes the neuron and brings about spontaneous HT bursting at ~6 Hz (middle trace). Reducing the concentration of *trans*-ACPD to 50 μM brings about a slow (<1 Hz) oscillation (bottom trace).

(B) Enlargement of a single HT burst (left) showing the presence of a fast afterdepolarization (ADP) (see further enlargement of boxed section in the inset). Enlargement of a single LTCP burst (center) showing the presence of smaller ISIs that increase as the burst progresses (the boxed section is further enlarged in the inset). Plots contrasting the averaged ISI patterns for intracellularly recorded HT- (●) and LTCP-mediated (□) bursts comprising 2, 3, 4, and 5 action potentials (far right).

(C) Spontaneous HT bursting in an LGN TC neuron in the presence of 100 μM trans-ACPD and 30 μM MPEP in the absence of injected DC current (top trace). 250 μM LY367385 initially brings about a spontaneous slow oscillation (15 min; middle trace) before leading simply to repetitive LTCP-mediated bursting (30 min; bottom left). The neuron now generates tonic firing following injection of depolarizing current and not HT bursting (30 min; bottom right). Data showing the induction of HT bursting via the physiological release of glutamate from corticothalamic fibers is shown in Supplemental Figure S4 at http://www.neuron.org/cgi/content/full/42/2/253/DC1. In this and subsequent figures, intracellularly recorded action potentials have been truncated for clarity.

intracellular recordings from morphologically identified TC neurons in LGN slices. In control conditions, these cells exhibited a resting membrane potential of −67 ± 1 mV and an apparent input resistance of 200 ± 14 MΩ (n = 206). Furthermore, all cells displayed characteristic LTCP-mediated bursting at hyperpolarized membrane potentials and sustained tonic firing in response to depolarization with injected DC current (Figure 3A, top traces). As shown previously (McCormick and Von Krosigk, 1992; Turner and Salt, 2000; Hughes et al., 2002b), *trans*-ACPD (100–150 μM) depolarized LGN TC neurons (ΔV = 16 ± 2 mV) and increased their apparent input resistance (309% ± 60%). In the majority of cases (n = 153 of 206; 74%), TC neurons continued to exhibit only tonic firing at depolarized membrane potentials following *trans*-ACPD application (data not shown). However, in the remainder of neurons (n = 53 of 206; 26%), action potential output at depolarized membrane potentials (>−55 mV) became characterized by spontaneous, repetitive HT bursting at ~2–13 Hz (1.9–13.9 Hz; n = 30) (Figure 3A, middle trace). In agreement with extracellular recordings (Figure 1A and Supplemental Figure S2A at http://www.neuron.org/cgi/content/full/42/2/253/DC1), application of a lower concentration of *trans*-ACPD (50 μM) could lead (n = 11 of 30; 37%) to a spontaneous slow (<1 Hz) oscillation (Hughes et al., 2002b) that was characterized by alternating "up" and "down" states and the generation of one or more LTCP-

mediated high-frequency bursts during the down state and at the transition stage from the down to up state (Figure 3A, bottom trace).

Intracellularly recorded HT bursts were essentially identical to extracellularly recorded bursts during in vitro α/θ oscillations since (1) they exhibited comparatively large ISIs (mean, 15.9 $\pm$ 0.8 ms; $p > 0.5$) that did not alter as the burst progressed (Figure 3B) and (2) the mean number of action potentials in a burst decreased as the interburst frequency increased such that, at an interburst frequency of 10 Hz or higher, all activity comprised either action potential doublets or occasional single spikes (see Figures 5A and 5B). Also in agreement with in vitro extracellular recordings, the frequency of HT bursting increased with increasing depolarization (Figure 5A) in the same range that in vitro α/θ oscillations occur (i.e., 2–13 Hz).

Similarly to in vitro extracellular field recordings, the actions of *trans*-ACPD in bringing about HT bursting (and the slow oscillation; see Hughes et al., 2002b) were emulated by DHPG (100 μM) (n = 2 of 8; 25%) but not by either the mGluR5 agonist CHPG (1 mM) (n = 8), the group II mGluR agonists APDC (100–200 μM) (n = 7) and DCG-IV (10–100 μM) (n = 7), or the group III mGluR agonist L-AP4 (100–200 μM) (n = 7) (data not shown). In addition, in the continual presence of 100–150 μM *trans*-ACPD, the mGluR1a antagonists LY367385 (250 μM) (n = 4) and CPCCOEt (300 μM) (n = 3) abolished HT bursting (Figure 3C) so that, in response to depolarizing DC current, neurons were only able to exhibit tonic firing (Figure 3C, bottom right trace). In contrast, the mGluR5 antagonist MPEP (30 μM) (n = 3) (Figure 3C), the group II mGluR antagonist EGLU (250 μM) (n = 3), and the group II/III mGluR antagonist CPPG (50 μM) (n = 3) were without effect (data not shown). mGluR1a-dependent HT bursting could also be elicited through the physiological release of glutamate via the stimulation of corticothalamic fibers (Supplemental Figure S4 at http://www.neuron.org/cgi/content/full/42/2/253/DC1).

Closely situated (<250 μm apart) simultaneous intra- and extracellular recordings of TC neuron activity in the presence of *trans*-ACPD (100–125 μM) (n = 5 of 27; 19%) confirmed that HT bursts were able to drive synchronized activity in the LGN slice (Figure 4). In these recordings, during periods when intracellularly recorded cells were hyperpolarized with injected DC current, no activity was evident in the extracellular recording (Figure $4A_1$). However, following the depolarization of the intracellularly recorded neuron and the induction of HT bursting, synchronized multiple unit activity was observed in the extracellular recording (Figures $4A_2$ and $4A_3$).

Ionic Mechanisms of HT Bursting

In other neuronal types, similar behavior to HT bursting is generated by a combination of Na^+ and Ca^{2+} channel activity (Magee and Carruth, 1999; Brumberg et al., 2000). We therefore investigated the effect of manipulating these ion channels on HT bursting. Application of tetrodotoxin (TTX) (1 μM) blocked the fast action potentials comprising the HT bursts but left intact an underlying oscillatory activity consisting of repetitive high-threshold (HT) spikes (Jahnsen and Llinás, 1984) (Figure 5A). The frequency of these HT spikes displayed an identical dependence on injected DC current to HT bursting apart from this dependence being positively shifted so that HT spikes occurred at more depolarized potentials (Figure 5C). In some TC neurons (n = 18 of 53; 34%), HT spikes were evident prior to TTX treatment where one or two such events marked the end of an HT burst (Figure 5E and Supplemental Figure S5A). HT bursts of this type were termed complex HT bursts.

HT spikes were unaffected by replacing extracellular Na^+ (n = 3) with choline ions but were reversibly abolished in all cases by removing extracellular Ca^{2+} (n = 4) or by applying 500 μM Co^{2+} (n = 4) (Supplemental Figure S5B at http://www.neuron.org/cgi/content/full/42/2/253/DC1). Surprisingly, HT spike amplitude was not significantly reduced by 300 μM Cd^{2+} (control, 25 $\pm$ 6 mV; 300 μM Cd^{2+}, 21 $\pm$ 8 mV; $p > 0.5$; n = 5), and even at 600 μM, Cd^{2+} did not fully block HT spike generation (control, 22 $\pm$ 1 mV; 600 μM Cd^{2+}, 12.3 $\pm$ 1.37 mV; $p < 0.01$; n = 5) (Supplemental Figure S5B). Accordingly, neither the L-type Ca^{2+} channel blocker nifedipine (10 μM) ($p > 0.1$; n = 3), the N/P/Q-type Ca^{2+} channel blocker ω-conotoxin-MVIIC (2–3 μM) ($p > 0.5$; n = 3), nor the N-type Ca^{2+} channel blocker ω-conotoxin-GVIA (2–3 μM) ($p > 0.5$; n = 3) significantly affected HT spike amplitude (Supplemental Figure S5B). In contrast, 300 μM Ni^{2+} was highly effective in reversibly suppressing HT spikes (control, 25 $\pm$ 5 mV; Ni^{2+}, 1 $\pm$ 1 mV; $p < 0.001$; n = 5) (Figure 5D and Supplemental Figure S5B). The effects of different Ca^{2+} channel blockers on HT bursts were in full agreement with their effects on HT spikes (see Supplemental Data and Supplemental Figure S5).

An additional characteristic feature of intracellularly recorded HT bursts was the presence of a fast afterdepolarization (ADP) that followed the action potentials comprising the burst (Figures 3B and 5F and Supplemental Figure S5A). This ADP was highly sensitive to TTX application, being abolished before a full block of the action potential was achieved (Figure 5F). However, the ADP was insensitive to the chelation of intracellular Ca^{2+} with either EGTA (50 mM) (n = 3) (Figure 5G) or BAPTA (50 mM) (n = 5), illustrating that it does not involve the activation of Ca^{2+}-dependent conductances.

In Vitro α/θ Oscillations Are Sensitive to Gap Junction Modulators

We next turned our attention to the way in which in vitro α/θ oscillations are synchronized between cells. Conventional chemical synaptic transmission was not required for their expression since they were routinely observed with quantitatively similar properties in the presence of blockers of non-NMDA, NMDA, $GABA_A$, and $GABA_B$ receptors (CNQX, 10 μM; DL-AP5, 100 μM; bicuculline, 30 μM, and CGP56999A, 10 μM, respectively) (n = 30) (Figures 6 and 9). In the light of this finding and the recent discovery of electrotonic and dye coupling between TC neurons (Hughes et al., 2002a), the effects of various gap junction modulators were tested on the properties of in vitro α/θ oscillations. Glycyrrhizic acid (GZA), the glycyrrhetinic acid derivative that is inactive as a gap junction blocker, did not affect either the frequency or peak power of the oscillations (n = 5) ($p > 0.5$) (Figures 6A, 6D, and 6E). However, the gap junction blockers carbenoxolone (CBX) (100–200 μM) (n = 7) (see

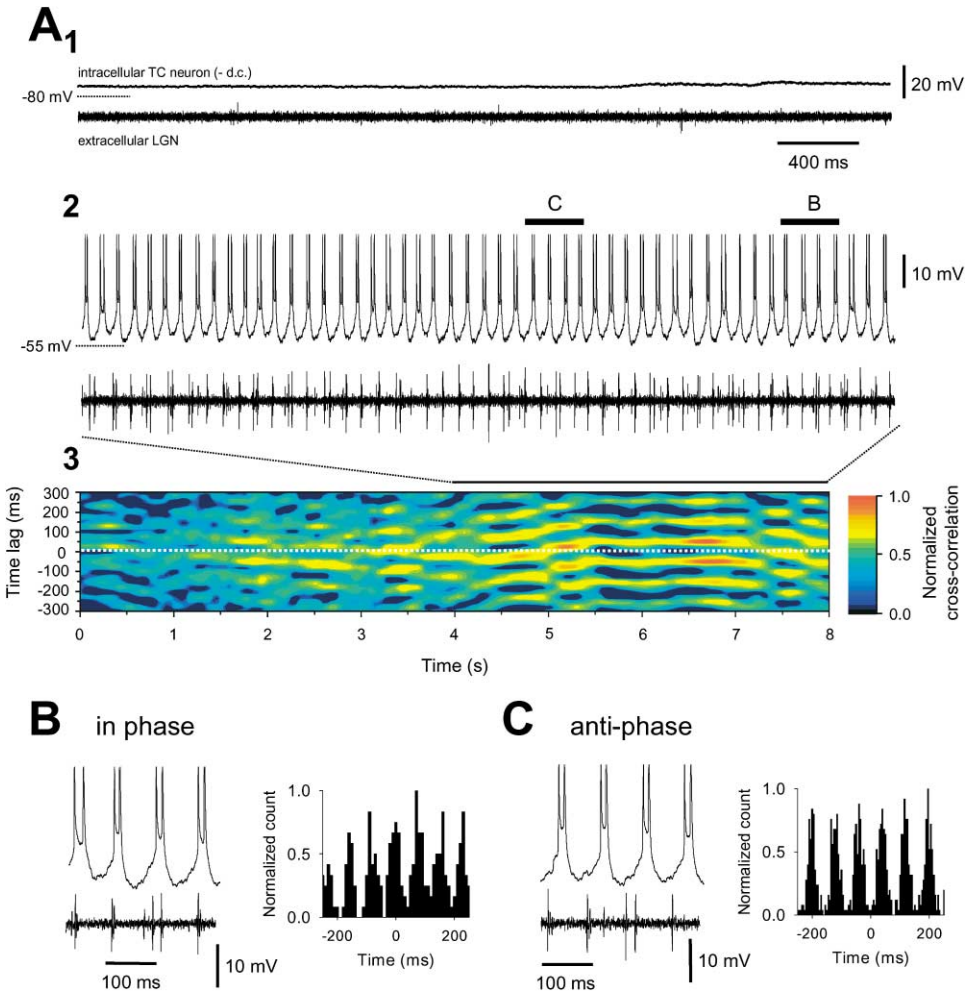

Figure 4. HT Bursting Drives Synchronized Activity in the LGN Slice

(A) HT burst generating LGN TC neuron held at −80 mV and a proximal (<250 μM) extracellular recording showing a lack of activity (1). When released from hyperpolarization, the intracellularly recorded neuron exhibits spontaneous HT bursting at ~12 Hz, which is accompanied by synchronized extracellular bursting in additional distinct cells (2). Sections marked B and C are expanded below. The image shows a discrete sliding window cross-correlogram of the intra- and extracellular recordings (3) (window duration, 400 ms; shift, 40 ms) with 0 ms corresponding to the initiation of bursting. Note how synchrony develops over a few seconds and can switch between in-phase and antiphase synchrony (see also Figure 9).

(B and C) Enlargement of episodes where the intra- and extracellular signals are in phase and antiphase, respectively, and the accompanying discrete cross-correlograms. (100 μM *trans*-ACPD was present during this experiment.)

also Figure 9A), 18β-glycyrrhetinic acid (18β-GA) (100 μM) (n = 6), oleamide (100 μM) (n = 5), and octanol (0.5 mM) (n = 6) reversibly depressed the peak power of in vitro α/θ oscillations to 18% ± 10% ($p < 0.001$), 7% ± 3% ($p < 0.001$), 10% ± 3% ($p < 0.001$), and 42% ± 11% ($p < 0.01$) of control values, respectively (Figures 6A, 6B, and 6D). Application of the putative gap junction opener trimethylamine (TMA) (20 mM) (n = 6) enhanced the peak power of in vitro α/θ oscillations by 255% ± 136% ($p < 0.001$), an effect that was reversibly attenuated by octanol application (0.5 mM) (n = 3) ($p < 0.01$) (Figure 6C and 6D).

Confirmation that HT Bursts Are Transmitted through Gap Junctions

We have previously shown that, following *trans*-ACPD application, around 20% of intracellularly recorded TC neurons display rhythmic spikelets (Figure 7A) which represent single action potentials transmitted through gap junctions during tonic firing (Hughes et al., 2002a). Since α/θ oscillations are (1) sensitive to gap junction blockers (Figure 6) and (2) associated with HT bursting in TC neurons rather than tonic firing (Figures 2 and 3), we might expect to observe some cells which exhibit "bursts of spikelets," which represent HT bursts transmitted through gap junctions and which would provide a clear substrate for the synchronization of α/θ oscillations. This was indeed the case with 11 out of 206 (5%) TC neurons exhibiting bursts of two to six spikelets for which we adopted the term burstlets (Figures 7B and 7C). Corresponding to HT bursts, which are manifested as either simple (comprising only a burst of action potentials, Figure 3B) or complex (consisting of a burst of action potentials followed by one or two slower HT spikes, Figure 5E) subtypes, two types of burstlets were observed: simple burstlets, comprising only two or more

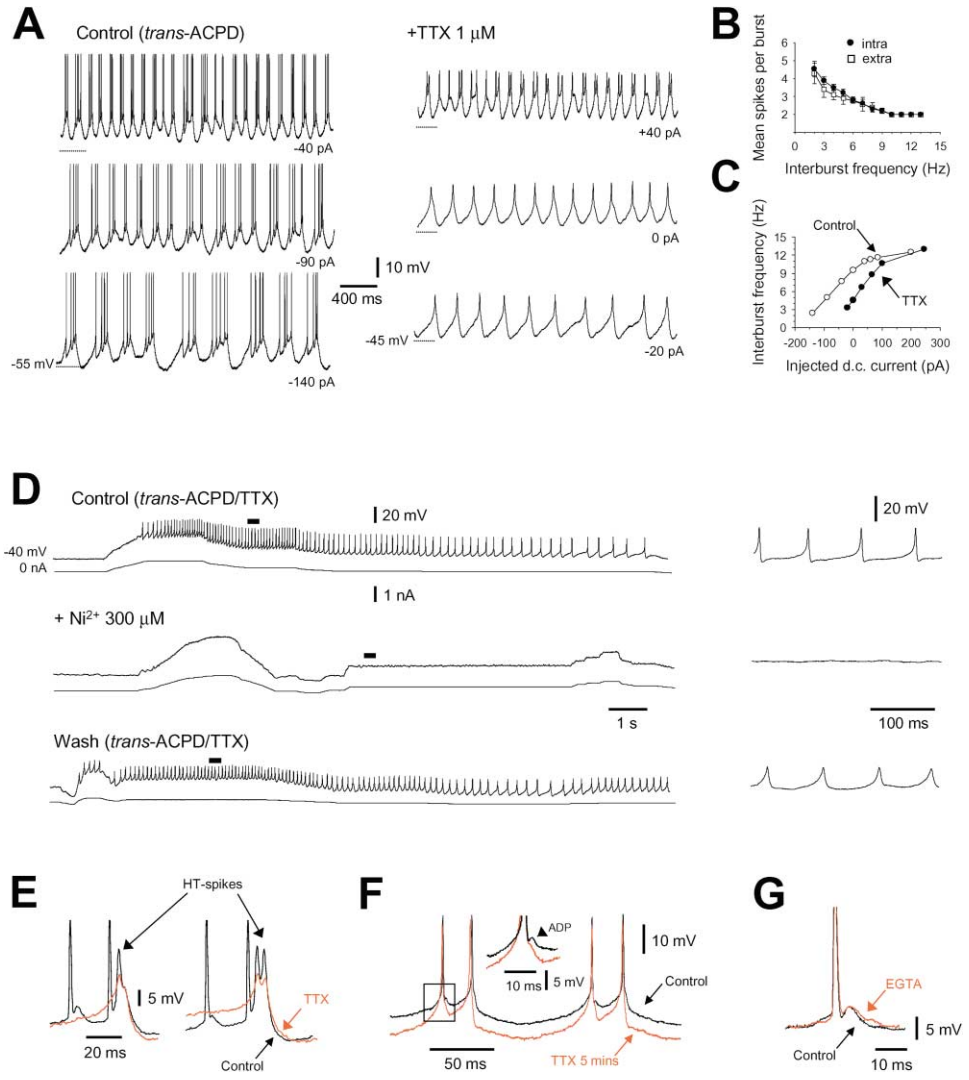

Figure 5. Properties and Mechanisms of HT Bursting in TC Neurons

(A) HT bursting at different levels of injected DC current showing an increase in interburst frequency with depolarization. TTX (1 μM) blocks the fast action potentials but leaves an oscillatory activity consisting of repetitive HT spikes intact.

(B) Plot of interburst frequency versus mean number of action potentials per HT burst (●) shows an identical profile to that for bursts recorded extracellularly during in vitro α/θ oscillations (□) (see Figure 2D).

(C) Plots of injected DC current versus interburst frequency before (○) and after (●) TTX application.

(D) A TC neuron in the presence of *trans*-ACPD (125 μM) and TTX (1 μM) exhibits repetitive HT spikes that are reversibly abolished by 300 μM Ni^{2+}. Sections marked by continuous lines are enlarged on the right.

(E) In some TC neurons, HT spikes are evident prior to TTX application (red line).

(F) The fast ADP is highly sensitive to TTX treatment and is abolished prior to a full block of the action potential.

(G) The ADP is unaffected by intracellular Ca^{2+} chelation following a 1 hr recording with an EGTA-filled electrode (50 mM). 100–125 μM *trans*-ACPD was present during all experiments depicted in this figure. Further information regarding the ionic mechanisms of HT bursting is shown in Supplemental Figure S5 at http://www.neuron.org/cgi/content/full/42/2/253/DC1.

spikelets (Figures 7B and 7E), or complex burstlets, appearing as a group of spikelets followed by one or two slower events (Figure 7C; arrowheads) (time to peak, 3.9 ± 0.9 ms; τ_{decay}, 3.4 ± 0.5 ms; n = 20). Simple burstlets accounted for 64% (n = 7 of 11) of cases, with complex burstlets making up the remainder (n = 4 of 11). In general, the majority of cells (8 of 11; 73%) where burstlets were observed also exhibited HT bursting so that 15% (8 of 53) of HT bursting TC neurons displayed both types of event.

The slower events present at the end of a complex burstlet were routinely observed following TTX application (Figure 7D) (n = 3) but were blocked by Ni^{2+} (250 μM) (n = 2 of 2), confirming that they represent HT spikes transmitted through gap junctions. These slower events were therefore termed HT spikelets. The mean ratio of HT spikelet to HT spike amplitude was 0.3 ± 0.04 (n = 3 cells), which was significantly larger than the mean ratio of spikelet to action potential amplitude 0.04 ± 0.004 (n = 10 cells) ($p < 0.001$).

As with isolated spikelets (Hughes et al., 2002a), burstlets were insensitive to a blockade of conventional

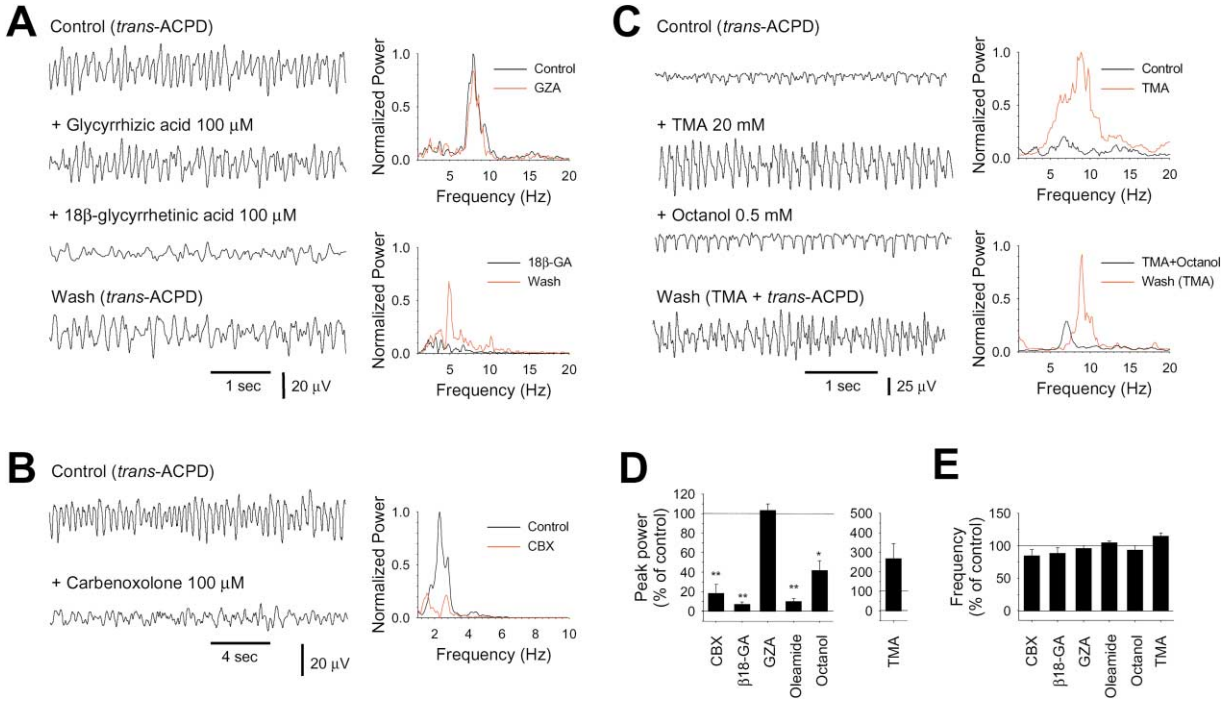

Figure 6. Suppression of In Vitro α/θ Field Oscillations by Gap Junction Blockers

(A) LGN field recording in the presence of 125 μM *trans*-ACPD showing synchronized activity at ~8 Hz (top trace). Application of glycyrrhizic acid (GZA) (100 μM) has no effect. However, application of the gap junction blocker 18β-glycyrrhetinic acid (18β-GA) (100 μM) abolishes the oscillation. Synchronized activity returns following washout of 18β-GA (bottom trace).

(B) LGN field oscillation at ~3 Hz recorded in the presence of 100 μM *trans*-ACPD (top trace). The oscillation is suppressed by 100 μM carbenoxolone (CBX) (bottom trace).

(C) LGN field recording in the presence of 125 μM *trans*-ACPD showing synchronized activity at ~7–9 Hz (top trace). Intracellular alkalinization via bath application of trimethylamine (TMA) (20 mM) greatly enhances the field oscillation, an effect that is reversibly inhibited by the gap junction blocker octanol (0.5 mM).

(D and E) Summary of the effects of various gap junction modulators on the peak power and frequency of α/θ field oscillations, respectively. 10 μM CNQX, 100 μM DL-AP5, 30 μM bicuculline, and 10 μM CGP56999A were present during all experiments depicted in this figure. *$p < 0.01$; **$p < 0.001$.

synaptic transmission with CNQX (10 μM), DL-AP5 (100 μM), bicuculline (30 μM), and CGP56999A (10 μM) ($n = 5$) but were abolished by CBX (100 μM) ($n = 3$) (Figure 7E). However, CBX did not block HT bursting (Figure 7E and Supplemental Figure S6) or affect apparent input resistance (data not shown). Further evidence that burstlets represent HT bursts transmitted through gap junctions was obtained by injecting dye into burstlet-generating cells and assessing whether additional cells were stained (i.e., dye coupling). Using this approach, we found that in 4 out of 5 (80%) cases, injection of the cellular marker biocytin led to dye coupling (Figure 7G). Dye coupling predominantly ($n = 3$ of 4; 75%) occurred between pairs of cells and not between more than four cells. Since, in general, dye coupling occurred in 39% ($n = 33$ of 85) of cases where TC neurons were injected with a marker, the probability that the association between burstlet generation and dye coupling occurred purely by chance was 0.07. The mean distance between dye-coupled TC neuron somas was 74 ± 9 μm ($n = 28$ pairs). Dye coupling was never observed when slices were continuously perfused with CBX (100 μM) ($n = 15$), with the probability of this occurring by chance being 0.0006.

The Properties of Burstlets and the Entrainment of TC Neuron Firing

The properties of burstlets corresponded exactly with those of HT bursts on a number of counts. First, burstlets occurred rhythmically in the same frequency range (1.8–12.5 Hz; $n = 9$) to HT bursts with interburstlet frequency but not burstlet amplitude, increasing with increasing depolarization (Figures 8A and 8B). Second, burstlets possessed relatively large interspikelet intervals (mean, 16.8 ± 0.9; $n = 63$) that did not alter as the burstlet progressed (Figure 8C) and which were not significantly different from the ISIs exhibited by HT bursts ($p > 0.5$). Third, the number of spikelets per burstlet decreased with increasing interburstlet frequency (Figure 8D) in a virtually identical way to that in which the number of action potentials per burst decreased with increasing interburst frequency for HT bursts.

At appropriate levels of membrane polarization, burstlets effectively entrained HT bursts leading to stable, phase-locked synchrony between the two events (Figure 8A). However, an increase in depolarization could disrupt this scenario and lead to a cycling between an in-phase and antiphase association (Figures 8E–8G). An identical cycling also occurred between simultane-

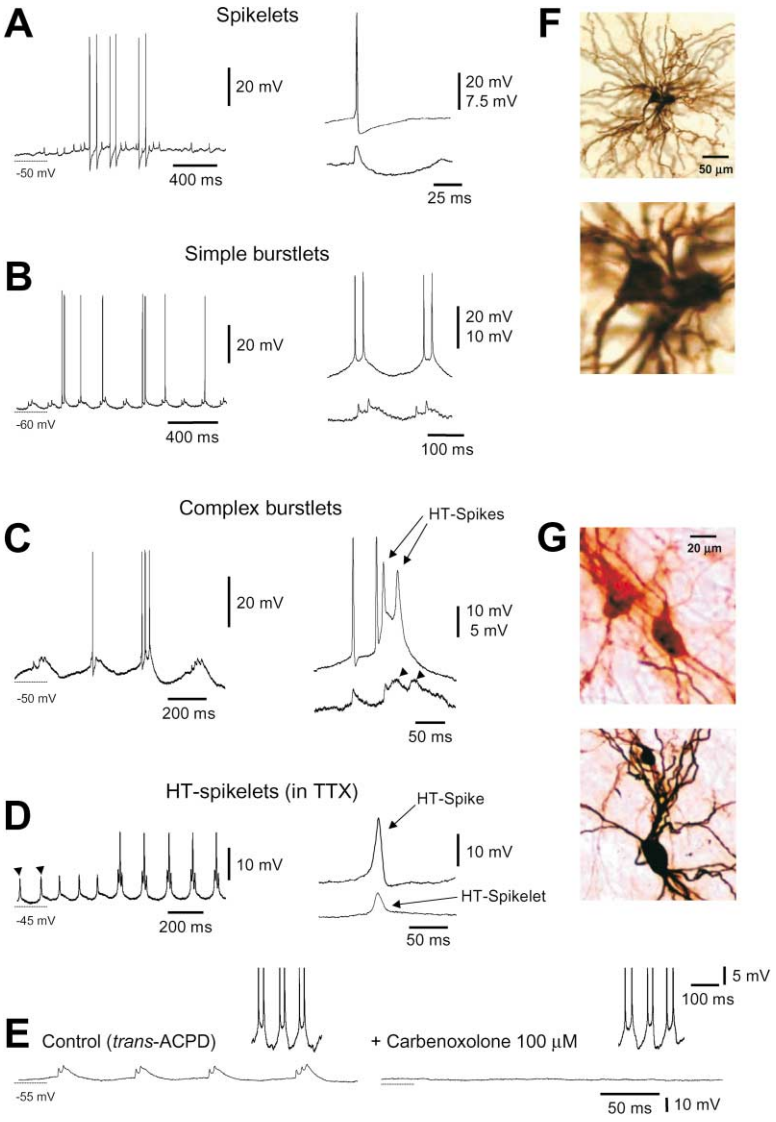

Figure 7. Transmission of TC Neuron Firing through Gap Junctions

(A) LGN TC neuron exhibiting rhythmic spikelets. The traces on the right show an enlarged action potential (top) and spikelet (bottom) from the same neuron. The time to peak of spikelets (1.7 ± 0.2 ms) was similar to that reported previously (Hughes et al., 2002a) and substantially longer than the time to peak of an action potential (0.65 ± 0.1 ms).

(B) LGN TC neuron exhibiting simple burstlets, i.e., groups of two or more spikelets only. The traces on the right show a comparison of two simple burstlets (bottom trace) with a pair of typical, simple HT bursts (top trace).

(C) LGN TC neuron exhibiting complex burstlets, i.e., a group of spikelets followed by one or two slower events (see arrowheads in enlargement, bottom right). The traces on the right show a comparison of a complex burstlet (bottom trace) with a typical, complex HT burst. The slower events (see arrowheads, bottom right) correspond well with the Ca^{2+}-dependent HT spikes that sometimes follow the action potentials in a complex HT burst (top trace, arrows).

(D) Spikelets are absent following TTX application but HT spikelets persist (arrowheads). The traces on the right show an enlarged comparison between an HT spike (top) and HT spikelet (bottom).

(E) Typical example of simple burstlets in a LGN TC neuron that are abolished following CBX application (100 μM). The insets show the accompanying lack of effect of CBX on HT bursting.

(F) Dye coupling obtained following biocytin injection into the neuron exhibiting spikelets shown in (A). An enlargement of the neuron somas is shown below.

(G) Dye coupling obtained following biocytin injection into the neuron exhibiting burstlets shown in (C). The image below shows an additional example of dye coupling obtained following biocytin injection into a TC neuron exhibiting burstlets. 100–150 μM *trans*-ACPD, 10 μM CNQX, 100 μM DL-AP5, 30 μM bicuculline, and 10 μM CGP56999A were present during the experiments depicted in this figure.

ously recorded extracellular units during α/θ field oscillations (n = 6) (Figure 9). In these recordings, prolonged periods were apparent where neurons fired synchronized bursts of action potentials in either an in-phase (Figure 9B) or antiphase manner (Figure 9C), with regular switching occurring between these two states. As observed with single-unit recordings (see Supplemental Figure S3), the phase changes in neuronal bursting that were observed in these recordings predictably affected the field oscillation amplitude so that, when a neuron switched to an in-phase relationship with the field oscillation, the oscillation amplitude was greater ($p < 0.001$). Importantly, application of CBX (100 μM) (n = 2) during multiunit recordings of phase-switching neurons greatly disrupted both the in-phase and antiphase states. This suggested that the phase-switching phenomenon was a direct result of gap junctional coupling and could therefore be completely attributed to the manner in which HT bursts and burstlets interact (Figure 8).

Discussion

This study shows that activation of mGluR1a in the isolated cat LGN induces synchronized oscillations at α (8–13 Hz) and θ (2–7 Hz) frequencies. These oscillations are driven by HT bursting, which occurs in a subset (~25%) of LGN TC neurons. HT bursting occurs at depolarized (> −55 mV) membrane potentials and is dependent on Ni^{2+}-sensitive Ca^{2+} channels. In vitro α/θ oscillations do not require conventional chemical synaptic transmission but rely on gap junctional coupling between LGN TC neurons. Our in vivo recordings identified a number of points of similarity between these in vitro α/θ oscillations and the thalamic α and θ waves that occur in vivo during relaxed wakefulness and early sleep, respectively. In combination with previous investigations (Whittington et al., 1995; Beierlein et al., 2000; Deans et al., 2001; Gillies et al., 2002; Long et al., 2004), these results indicate that activation of mGluRs is an

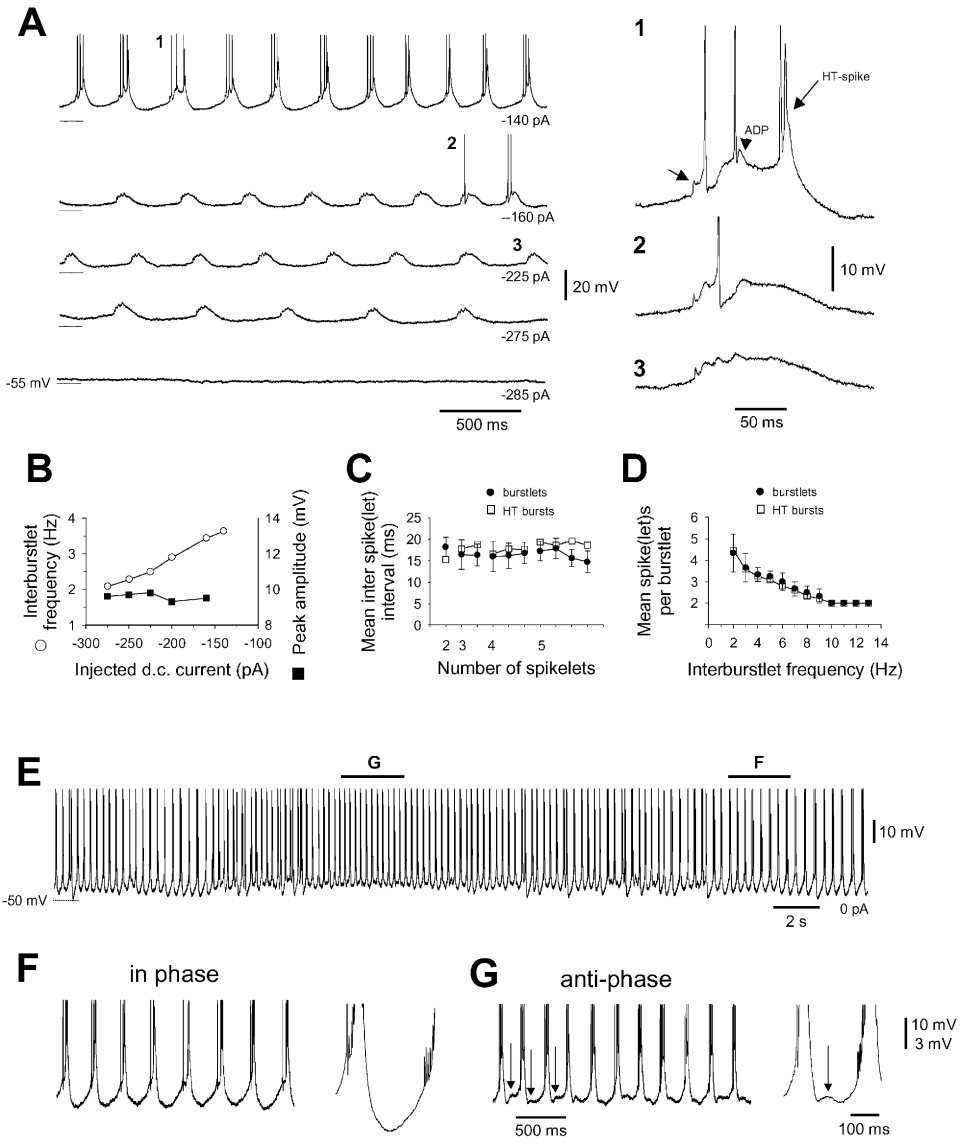

Figure 8. Properties of Burstlets in TC Neurons

(A) Activity of a LGN TC neuron exhibiting complex burstlets at various levels of injected DC current. Burstlet frequency increases with increasing depolarization eventually triggering full-blown HT bursts on every cycle (top trace). Events marked 1, 2, and 3 are enlarged on the right. The top right trace (1) shows an enlargement of a burstlet leading to a full-blown HT burst. The trace below (2) shows a burstlet leading to a single action potential. The bottom trace (3) shows an isolated burstlet.

(B) Plot of injected DC current versus interburstlet frequency (○) and peak burstlet amplitude (■).

(C) Averaged interspikelet interval patterns for burstlets comprising 2, 3, and 4 spikelets are similar to the ISI patterns of intra- and extracellularly recorded HT bursts (averaged together and plotted as □).

(D) Plot of interburstlet frequency versus number of spikelets per burstlet (●) shows identical properties to the average values for pooled intra- and extracellularly recorded HT bursts (□).

(E) Activity of the neuron depicted in (A) over a longer time course and at a more depolarized level. Sections marked F and G are expanded below.

(F) During this period, the voltage waveform between HT bursts is smooth, suggesting that HT bursts and burstlets are in phase (see [A], top trace). The trace on the right shows the averaged interburst interval.

(G) During this period, the voltage waveform between HT bursts is interrupted by small depolarizations (arrows) that indicate a disruption of the phase relationship between HT bursts and burstlets. The averaged interburst interval (right) shows an antiphase depolarization between the bursts (arrow).

important general mechanism for inducing physiologically relevant, synchronized oscillations in a variety of brain areas. In particular, we suggest that mGluR1a-induced α/θ oscillations are a possible mechanism by which the thalamus could promote EEG α and θ activity in the intact brain.

HT Bursting as the Driving Force for α/θ Oscillations

The driving force behind in vitro α/θ oscillations is an unusual form of burst firing termed HT bursting. HT bursting is caused by an underlying membrane potential oscillation comprising regenerative HT spikes and is

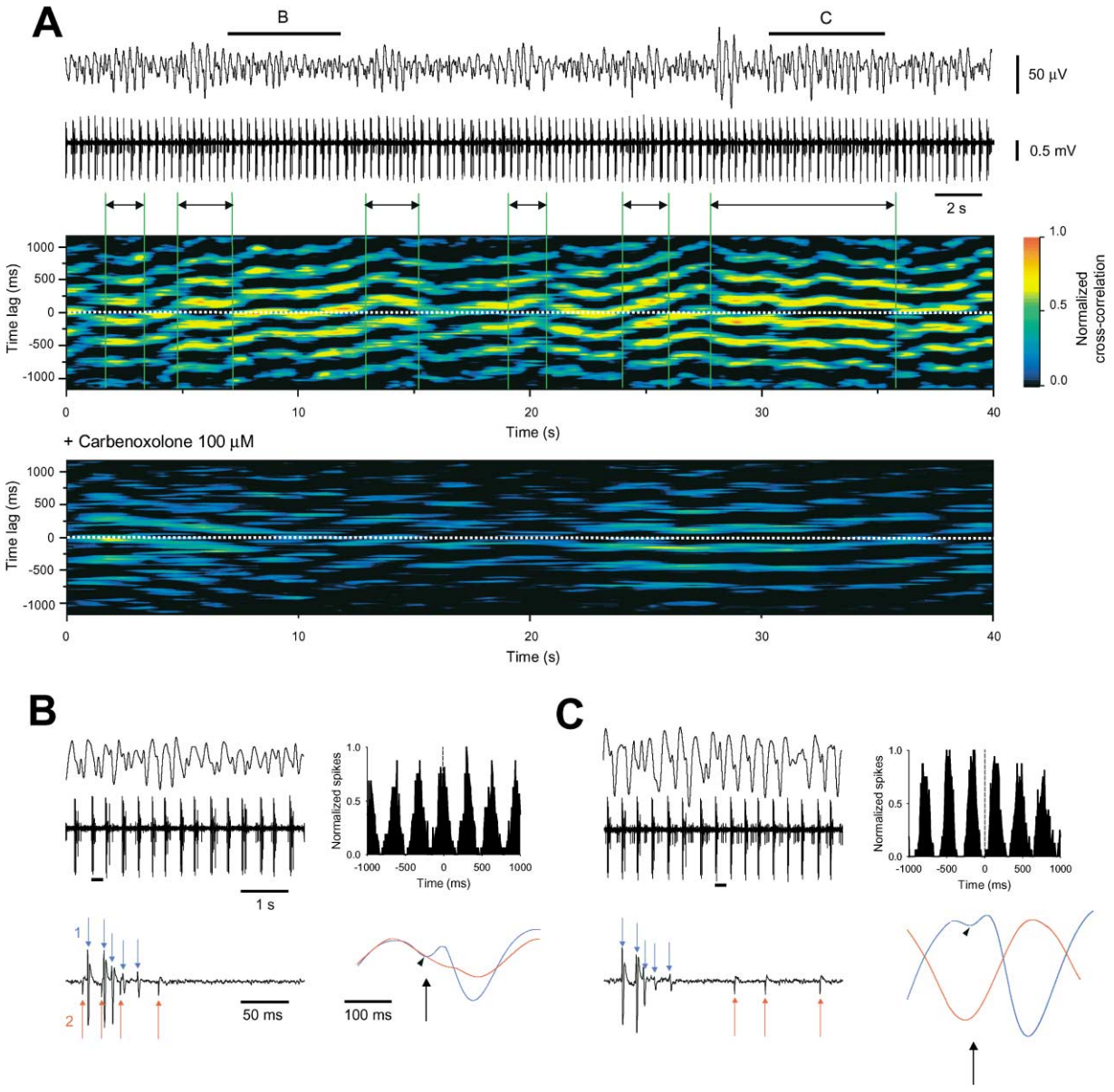

Figure 9. Phase Switching during In Vitro α/θ Field Oscillations and the Effect of Carbenoxolone on Multiunit Activity

(A) Simultaneous LGN field (top trace) and double-unit (bottom trace) recording in the presence of 100 μM *trans*-ACPD. Sliding window cross-correlogram of the two units (shown below) reveals dynamic switching between approximately in-phase and antiphase firing (window duration, 1500 ms; shift, 150 ms). Large-amplitude waves in the field recording correspond with periods of antiphase synchrony between the two units (see double-headed arrows). The additional sliding window cross-correlogram shows how synchrony between the units is greatly disrupted by 100 μM carbenoxolone.

(B) Enlargement of the in-phase period marked by B in (A) and the accompanying discrete cross-correlogram (right). Below, an enlargement of the underlined section shows the presence of the two units in synchrony. The field oscillation averages using the first action potential in the burst of unit 1 (blue trace) and 2 (red trace) as a reference (see arrow) are shown on the right. Both units are out of phase with the negative peak of the field oscillation. Note the presence of a smaller antiphase wave in the blue trace (see arrowhead).

(C) Enlargement of the out-of-phase period marked by C in (A) and the accompanying discrete cross-correlogram (right). Below, an enlargement of the underlined section shows the two units firing out of phase. Field oscillation averages using the first action potential in the burst of unit 1 (blue trace) and 2 (red trace) as reference (see arrow) are shown on the right. Unit 1 remains out of phase with the peak of the field oscillation while unit 2 is in phase. Note the greater amplitude of the main field oscillation. 100 μM *trans*-ACPD, 10 μM CNQX, 100 μM DL-AP5, 30 μM bicuculline, and 10 μM CGP56999A were present during this recording.

distinct to the well-characterized LTCP-mediated bursting that is correlated with slow (<1 Hz) sleep wave activity. Previously, HT spikes have mainly been observed following a pharmacological blockade of K^+ channels with 4-aminopyridine (4-AP) (Jahnsen and Llinás, 1984; see also the Supplemental Data at http://www.neuron.org/cgi/content/full/42/2/253/DC1) and have therefore been thought to represent dendritic spikes that can only

be expressed following a reduction in dendritic K^+ conductance. Our data are consistent with this, since it is well known that mGluRs on TC neurons are located at distal sites (Godwin et al., 1996) and that their activation decreases K^+ conductance (McCormick and Von Krosigk, 1992) of probable dendritic location (Zhan et al., 2000). However, while 4-AP-induced HT spikes seem to be a general characteristic of TC neurons in a variety of sensory nuclei (Jahnsen and Llinás, 1984; see also the Supplemental Data), we only observed *trans*-ACPD-dependent HT bursting in a subpopulation of LGN TC neurons. Hence, why some TC neurons tend to exhibit HT bursts while others do not could be due to a number of factors, including differences in K^+ channel expression and mGluR effects, and is yet to be ascertained.

Consistent with earlier studies (Jahnsen and Llinás, 1984), HT spikes were found to be generated by voltage-dependent Ca^{2+} channels. However, both HT spikes and HT bursting were more sensitive to Ni^{2+} than to Cd^{2+} and specific high-voltage-activated Ca^{2+} channel blockers, suggesting that they are dependent on T-type Ca^{2+} channels (see also Gillies et al., 2002). While this may seem surprising, it is a finding that is well supported by a recent study in the rat LGN showing that the distal dendrites of TC neurons express T-type Ca^{2+} channels that (1) exhibit steady-state activation and inactivation curves that are depolarized by ~10 mV compared to T-type channels near the soma and (2) can generate isolated depolarizing potentials independently of more proximal T-type channels (Williams and Stuart, 2000).

α/θ Oscillations Are Synchronized by Electrical Coupling between TC Neurons

Conventional synaptic transmission is not critical for the generation of in vitro α/θ oscillations, as they were observed in the presence of GABAergic and ionotropic glutamatergic receptor blockers. However, thalamic α/θ oscillations were diminished by gap junction blockers and were enhanced by intracellular alkalinization via TMA application. Notwithstanding the nonspecific nature of these compounds (Rozental et al., 2001) and while acknowledging a possible contribution from conventional chemical synapses and, in particular, from inhibitory thalamic neurons (Zhu et al., 1999; Long et al., 2004), their common action in modulating electrical coupling endorses the view that α/θ oscillations are largely coordinated by gap junctional coupling. The presence of burstlets in intracellular recordings of TC neurons and the way in which burstlets and HT bursts interact provide a clear substrate for the synchronization of α/θ oscillations. Nine lines of evidence support the conclusion that burstlets represent HT bursts transmitted through gap junctions or, more explicitly, that HT bursting TC neurons are DC coupled by intercellular channels. First, burstlets comprise groups of spikelets which have identical properties to those shown to represent electrotonically transmitted action potentials (Hughes et al., 2002a). Second, burstlets are regularly accompanied by dye coupling. Furthermore, this dye coupling is unlikely to be artifactual, since it is always restricted to a few neurons, does not involve other cell types (e.g., glial cells), is much less likely when burstlets (or isolated spikelets) are not present, and is absent when slices are bathed in CBX. Third, burstlets are abolished by CBX but are unaffected by blocking conventional synaptic transmission. Fourth, burstlets occur rhythmically in the same frequency range as HT bursts. Fifth, the relationship between burstlets and spikelets is identical to that between HT bursts and action potentials. Sixth, 34% of HT-bursting TC neurons show complex bursts, while 27% of burstlet-generating TC neurons exhibit complex burstlets. Seventh, the slower events present at the end of a complex burstlet are resistant to TTX but blocked by Ni^{2+}, confirming that they represent residual HT spikes transmitted through gap junctions. Eighth, the frequency but not the amplitude of burstlets is sensitive to membrane polarization. Ninth, as shown in several theoretical studies examining the properties of excitable cells coupled by gap junctions (e.g., Sherman and Rinzel, 1992; Cymbalyuk et al., 1994), HT bursts and burstlets can exhibit both an in-phase and antiphase relationship, with spontaneous shifts regularly occurring between these two states.

As implied earlier (Hughes et al., 2002a), and since (1) dye coupling rarely occurs between more than two TC neurons and (2) DC current injection into a TC neuron exhibiting burstlets can easily modify interburstlet frequency, it appears that, although strongly coupled, TC neurons are not extensively interconnected by gap junctions as in other brain areas (Galarreta and Hestrin, 1999; Gibson et al., 1999; Deans et al., 2001). While it may seem that such a sparse connectivity would be unable to support physiologically relevant network oscillations, the opposite has been shown for the involvement of hippocampal pyramidal neurons in ultrafast (~180–200 Hz) oscillations or so-called ripples (Draguhn et al., 1998). This is because a higher density of connections than ~2.5–3 per cell leads to continuous firing and therefore cannot support the dynamic features of ripple oscillations, i.e., occurrence in transient episodes (Traub and Bibbig, 2000). In a similar way, we suspect that a more dense interconnectivity between TC neurons would prevent the phase shifting that occurs during in vitro α/θ oscillations and would therefore be unable to support the dynamic waxing and waning of these oscillations as described in this study. Indeed, sparse connectivity may be an important general principle regarding electrical connections between excitatory neurons in the mature CNS, which supports controlled and responsive oscillatory states as opposed to pathological hypersynchrony.

The Relevance of In Vitro α/θ Oscillations to EEG α and θ Rhythm Generation In Vivo

Recent studies suggest that gap junctional coupling in the CNS seems to be largely restricted to the connection of similar cell types within the same nucleus (Gibson et al., 1999; Galarreta and Hestrin 1999; Long et al., 2004; see also Venance et al., 2000), while both short- and long-range internuclear connections appear to be the exclusive remit of chemical synapses. Thus, in vitro investigations, which tend to isolate individual nuclei for experimentation, may disproportionately highlight the role of gap junctions in generating synchronized oscillations in comparison to longer range chemical interactions. As such, some caution should be exercised when translating our in vitro results to the in vivo scenario.

Nevertheless, our in vivo experiments highlight a number of points of correspondence between in vivo thalamic α and θ rhythms and in vitro α/θ oscillations. First, in both cases, the oscillations require the activation of mGluR1a. Although the site of action of i.v. injected mGluR antagonists in the intact brain will clearly not be restricted to the thalamus, it remains that mGluR1a activation is specifically involved in supporting α rhythm generation in both scenarios. Second, the bursting that occurs in a subset of TC neurons during in vitro α/θ oscillations is similar to that which we observed in vivo (see also Bouyer et al., 1982; Buzsáki, 1991). Whether or not the same mechanisms are responsible for this activity in both contexts, however, is yet to be determined. Third, as excitability is reduced in the LGN slice by decreasing the intensity of mGluR1a activation, we observed a progressive change from α to θ oscillations followed by the appearance of biphasic slow ($<$1 Hz) waves. Similar changes occur in vivo as arousal is diminished from relaxed wakefulness, through drowsiness, to deep sleep. Of course, we do not suggest that EEG α and θ (and slow) rhythms in the intact brain are a simple reflection of synchronized oscillations in the thalamus nor that the transition between these activities is purely determined by the level of thalamic mGluR activation. Indeed, other brain areas, particularly cortical circuits (Lopes da Silva et al., 1980; Silva et al., 1991; Liley et al., 1999), and additional neuromodulatory systems, especially those arising in the brainstem and hypothalamus (McCormick, 1992), undoubtedly also play important roles. Be that as it may, we propose that the in vitro α/θ oscillations described in this study are a candidate mechanism by which the thalamus could support the generation of EEG α and θ rhythms in the intact brain.

Experimental Procedures

In vivo experiments were carried out in accordance with local ethical committee guidelines and the Hungarian Act of Animal Care and Experimentation (1998. XXVIII. Section 243/1998), which conforms to the European Community regulations (86/609/). In vitro procedures involving experimental animals were carried out in accordance with local ethical committee guidelines and the UK Animals (Scientific Procedure) Act, 1986. All efforts were made to minimize the suffering and number of animals used in each experiment.

In Vitro Slice Preparation and Maintenance

Young adult cats (1–1.5 kg) were deeply anesthetized with a mixture of O_2 and NO_2 (2:1) and 2.5% halothane, a wide craniotomy performed, and the brain removed. Coronal or sagittal slices of the thalamus containing the dorsal lateral geniculate nucleus (LGN) were prepared and maintained as described previously (Hughes et al., 2002a, 2002b). For recording, slices (450–500 μm) were perfused with a warmed (35°C $\pm$ 1°C) continuously oxygenated (95% O_2, 5% CO_2) artificial cerebrospinal fluid (ACSF) containing (in mM) NaCl (134), KCl (2), KH_2PO_4 (1.25), $MgSO_4$ (1), $CaCl_2$ (2), $NaHCO_3$ (16), and glucose (10). For experiments involving $CoCl_2$, $NiCl_2$, or $CdCl_2$, $MgSO_4$ was replaced with $MgCl_2$, and KH_2PO_4 was omitted. Oleamide and nifedipine were dissolved in 100% ethanol and added to the final solution such that the final total volume of ethanol did not exceed 0.1%. Experiments involving the addition of nifedipine were performed in semidarkness. 18β-glycyrrhetinic acid and glycyrrhizic acid were dissolved in DMSO solution such that the final total volume of DMSO did not exceed 0.1%. All other drugs were dissolved directly in ACSF. For the sources and full names of the drugs, see the Supplemental Data at http://www.neuron.org/cgi/content/full/42/2/253/DC1.

In Vitro Electrophysiology

Extracellular recordings were performed using glass pipettes filled with 0.5 M NaCl (resistance, 1–5 MΩ) connected to a Neurolog 104 differential amplifier (Digitimer Ltd., Welwyn Garden City, UK). Field and unit activities were simultaneously recorded through the same electrode by band-pass filtering at 1–15 Hz (0.1–2 Hz for slow waves) and 0.1–20 kHz, respectively. Intracellular recordings, using the current clamp technique, were performed with standard-wall glass microelectrodes filled with 1 M potassium acetate (resistance, 80–120 MΩ) and, in some cases, 2% biocytin or neurobiotin and connected to an Axoclamp-2A amplifier (Axon Instruments, Foster City) operating in bridge mode. Impaled cells were identified as TC neurons using established electrophysiological and morphological criteria (Hughes et al., 2002b). In slices where neurons had been filled with biocytin, visualization of the dye was performed as described previously (Hughes et al., 2002a).

In Vitro Data Analysis

Voltage and current records were stored on a Biologic DAT recorder (IntraCel, Royston, UK) and later analyzed using Clampfit (Axon Instruments). Apparent input resistance (R_N) was estimated from voltage responses evoked at $-$60 mV by small (20–50 pA) hyperpolarizing current steps. Statistical significance was assessed using Student's t test. Normalized discrete cross-correlograms of two spike trains were constructed by computing the intervals between the times of all spikes in one train and all spikes in the other. Intervals were then binned at 5 or 10 ms. The resulting histogram was then normalized by dividing all entries by the peak value. Each time slice of a discrete sliding window cross-correlogram represents a normalized discrete cross-correlogram corresponding to a given window centered around that time. Consecutively shifting this window by a uniform time interval generates a matrix of values which were color coded to produce the final image. The probability that a particular frequency of dye coupling occurred in association with certain conditions purely by chance was calculated according to the method described in Hughes et al. (2002a). All quantitative results are expressed as mean $\pm$ SEM.

Surgery and Implantation for Chronic Recordings

Adult cats (3.2–4.5 kg) were anesthetized with 40 mg/kg Nembutal and placed into a stereotaxic frame (David Kopf 900 series, David Kopf Instruments, Tujunga). Stainless steel screws (0.6 mm) were implanted above the occipital and parietal cortices for EEG recording. In addition, two screws were placed into the orbital bone to record EOG, and a pair of stainless steel wire electrodes were inserted into the neck muscles for EMG recording. Bilateral 3 mm holes were drilled into the bone for implanting electrode arrays (see below) at coordinates A, 7.2; L, 9.5–10; V, +6 mm (Berman and Jones, 1982). A small intravenous cannula was then inserted into the right jugular vein, and its Leuer lock cone was cemented to the skull. The cannula was filled with a heparin-saline solution (10% heparin in saline) which was changed daily. Cats were allowed to recover from the implantation for at least 5 days before recording commenced, and during this period they were moved (once a day) to the recording chamber for habituation to the environment and the connecting cable. At the end of the experiment, animals were given a lethal injection of Nembutal, placed in a stereotaxic frame, and the electrode tip positions surgically verified in situ.

In Vivo Recording

For simultaneous recording of field and single units in the LGN, we used custom-made electrode arrays comprising two microelectrodes for recording unit activity and an additional electrode for local field potentials separated by a distance of 400 μm. Microelectrodes were made of electrolythically edged tungsten wires of 80 μm diameter and had an impedance of 300–400 kΩ. For recording local field potentials, we also used electrolythically edged tungsten electrodes that were hand scraped to 10 kΩ after insulation. Each electrode array was attached to the piston of a cylinder-piston-type microdrive and implanted (as described earlier, Juhász et al., 1986) so that the

electrode tips were initially 2 mm above the LGN. On the first day of the experiments, cats were moved to a sound-proofed and electrically shielded chamber with a Plexiglas front window. Stages of vigilance were estimated using standard criteria on the basis of polygraphic (EEG, EOG, and EMG) recordings with a Grass 8B EEG amplifier (Grass Instruments) which were sampled with a CED 1401 (Cambridge Electronic Design Ltd., Cambridge, UK) and stored on a personal computer for offline analysis. Extracellular unit activity was simultaneously recorded by a Supertech Bioamp preamplifier (Supertech, Pécs, Hungary) with an input impedance of 10 MΩ and band-pass filtered at 500 Hz to 10 kHz. Additional information regarding in vivo recordings is given in the Supplemental Data at http://www.neuron.org/cgi/content/full/42/2/253/DC1.

Acknowledgments

We wish to thank Dr T.I. Tóth for helpful discussions during the course of this study and Mr. T.M. Gould for technical assistance. This work was supported by the Wellcome Trust (grant 71436), OTKA TS044711, and MEDICHEM 8_11. K.A.K. was the recipient of a Bolyai Grant. Additional information regarding this and other published work from the Crunelli lab is available at http://www.thalamus.org.uk.

Received: April 25, 2003
Revised: December 5, 2003
Accepted: March 10, 2004
Published: April 21, 2004

References

Amzica, F., and Steriade, M. (1998). Cellular substrates and laminar profile of sleep K-complex. Neuroscience *82*, 671–686.

Beierlein, M., Gibson, J.R., and Connors, B.W. (2000). A network of electrically coupled interneurons drives synchronized inhibition in neocortex. Nat. Neurosci. *3*, 904–910.

Berger, H. (1933). Über das Elektrenkephalogramm des Menschen Siebente Mitteilung (7th report). Arch. Psychiat. Nervenkr. *103*, 444–454.

Berman, A.L., and Jones, E.G. (1982). The Thalamus and Basal Telencephalon of the Cat (Madison, WI: The University of Wisconsin Press).

Bouyer, J.J., Rougeul, A., and Buser, P. (1982). Somatosensory rhythms in the awake cat: a single unit exploration of their thalamic concomitant in nucleus ventralis posterior and vicinity. Arch. Ital. Biol. *120*, 95–110.

Bouyer, J.J., Tilquin, C., and Rougeul, A. (1983). Thalamic rhythms in cat during quiet wakefulness and immobility. Electroencephalogr. Clin. Neurophysiol. *55*, 180–187.

Brumberg, J.C., Nowak, L.G., and McCormick, D.A. (2000). Ionic mechanisms underlying repetitive high-frequency burst firing in supragranular cortical neurons. J. Neurosci. *20*, 4829–4843.

Buzsáki, G. (1991). The thalamic clock: emergent network properties. Neuroscience *41*, 351–364.

Buzsáki, G. (2002). Theta Oscillations in the Hippocampus. Neuron *33*, 325–340.

Chatila, M., Milleret, C., Rougeul, A., and Buser, P. (1993). Alpha rhythm in the cat thalamus. C. R. Acad. Sci. III *316*, 51–58.

Cymbalyuk, G.S., Nikolaev, E.V., and Borisyuk, R.M. (1994). In-phase and antiphase self-oscillations in a model of two electrically coupled pacemakers. Biol. Cybern. *71*, 153–160.

Danos, P., Guich, S., Abel, L., and Buchsbaum, M.S. (2001). EEG alpha rhythm and glucose metabolic rate in the thalamus in schizophrenia. Neuropsychobiology *43*, 265–272.

Deans, M.R., Gibson, J.R., Sellitto, C., Connors, B.W., and Paul, D.L. (2001). Synchronous activity of inhibitory networks in neocortex requires electrical synapses containing connexin36. Neuron *31*, 477–485.

Draguhn, A., Traub, R.D., Schmitz, D., and Jefferys, J.G. (1998). Electrical coupling underlies high-frequency oscillations in the hippocampus in vitro. Nature *394*, 189–192.

Galarreta, M., and Hestrin, S. (1999). A network of fast-spiking cells in the neocortex connected by electrical synapses. Nature *402*, 72–75.

Gibson, J.R., Beierlein, M., and Connors, B.W. (1999). Two networks of electrically coupled inhibitory neurons in neocortex. Nature *402*, 75–79.

Gillies, M.J., Traub, R.D., LeBeau, F.E.N., Davies, C.H., Gloveli, T., Buhl, E.H., and Whittington, M.A. (2002). A model of atropine-resistant theta oscillations in rat hippocampal area CA1. J. Physiol. *543*, 779–793.

Godwin, D.W., Van Horn, S.C., Eriir, A., Sesma, M., Romano, C., and Sherman, S.M. (1996). Ultrastructural localization suggests that retinal and cortical inputs access different metabotropic glutamate receptors in the lateral geniculate nucleus. J. Neurosci. *16*, 8181–8192.

Goldman, R.I., Stern, J.M., Engel, J., Jr., and Cohen, M.S. (2002). Simultaneous EEG and fMRI of the alpha rhythm. Neuroreport *13*, 2487–2492.

Hughes, S.W., Blethyn, K.L., Cope, D.W., and Crunelli, V. (2002a). Properties and origin of spikelets in thalamocortical neurons in vitro. Neuroscience *110*, 395–401.

Hughes, S.W., Cope, D.W., Blethyn, K.L., and Crunelli, V. (2002b). Cellular mechanisms of the slow (<1 Hz) oscillation in thalamocortical neurons in vitro. Neuron *33*, 947–58 (2002b).

Jahnsen, H., and Llinás, R. (1984). Ionic basis for the electro-responsiveness and oscillatory properties of guinea-pig thalamic neurones in vitro. J. Physiol. *349*, 227–247.

Juhász, G., Détári, L., and Kukorelli, T. (1986). Effects of hypnogenic vagal stimulation on thalamic neuronal activity in cats. Brain Res. Bull. *15*, 437–441.

Kanamori, N. (1993). Rhythmic slow waves of lateral geniculate nucleus in the cat: relation to vigilance. Int. J. Neurosci. *68*, 117–122.

Larson, C.L., Davidson, R.J., Abercrombie, H.C., Ward, R.T., Schaefer, S.M., Jackson, D.C., Holden, J.E., and Perlman, S.B. (1998). Relations between PET-derived measures of thalamic glucose metabolism and EEG alpha power. Psychophysiology *35*, 162–169.

Liley, D.T., Alexander, D.M., Wright, J.J., and Aldous, M.D. (1999). Alpha rhythm emerges from large-scale networks of realistically coupled multicompartmental model cortical neurons. Network *10*, 79–92.

Lindgren, K.A., Larson, C.L., Schaefer, S.M., Abercrombie, H.C., Ward, R.T., Oakes, T.R., Holden, J.E., Perlman, S.B., Benca, R.M., and Davidson, R.J. (1999). Thalamic metabolic rate predicts EEG alpha power in healthy control subjects but not in depressed patients. Biol. Psychiatry *45*, 943–952.

Long, M.A., Lanmdisman, C.E., and Connors, B.W. (2004). Small clusters of electrically coupled neurons generate synchronous rhythms in the thalamic reticular nucleus. J. Neurosci. *24*, 341–349.

Lopes da Silva, F.H., van Lierop, T.H., Schrijer, C.F., and van Leeuwen, W.S. (1973). Organization of thalamic and cortical alpha rhythms: spectra and coherences. Electroencephalogr. Clin. Neurophysiol. *35*, 627–639.

Lopes da Silva, F.H., Vos, J.E., Mooibroek, J., and Van Rotterdam, A. (1980). Relative contributions of intracortical and thalamo-cortical processes in the generation of alpha rhythms, revealed by partial coherence analysis. Electroencephalogr. Clin. Neurophysiol. *50*, 449–456.

Magee, J.C., and Carruth, M. (1999). Dendritic voltage-gated ion channels regulate the action potential firing mode of hippocampal CA1 pyramidal neurons. J. Neurophysiol. *82*, 1895–1901.

McCarley, R.W., Benoit, O., and Barrionuevo, G. (1983). Lateral geniculate nucleus unitary discharge in sleep and waking: state- and rate-specific aspects. J. Neurophysiol. *50*, 798–818.

McCormick, D.A. (1992). Neurotransmitter actions in the thalamus and cerebral cortex and their role in neuromodulation of thalamocortical activity. Prog. Neurobiol. *39*, 337–388.

McCormick, D.A., and von Krosigk, M. (1992). Corticothalamic acti-

vation modulates thalamic firing through glutamate "metabotropic" receptors. Proc. Natl. Acad. Sci. USA *89*, 2774–2778.

Niedermeyer, E. (1993a). The normal EEG of the waking adult. In Electroencephalography: Basic Principles, Clinical Applications, and Related Fields, E. Niedermeyer and F. Lopes da Silva, eds. (Baltimore: Williams and Wilkins), pp. 97–117.

Niedermeyer, E. (1993b). Sleep and EEG. In Electroencephalography: Basic Principles, Clinical Applications, and Related Fields, E. Niedermeyer and F. Lopes da Silva, eds. (Baltimore: Williams and Wilkins), pp. 153–191.

Rougeul-Buser, A., and Buser, P. (1997). Rhythms in the alpha band in cats and their behavioural correlates. Int. J. Psychophysiol. *26*, 191–203.

Rozental, R., Srinivas, M., and Spray, D.C. (2001). How to close a gap junction channel. Efficacies and potencies of uncoupling agents. Methods Mol. Biol. *154*, 447–76.

Sherman, A., and Rinzel, J. (1992). Rhythmogenic effects of weak electrotonic coupling in neuronal models. Proc. Natl. Acad. Sci. USA *89*, 2471–2474.

Silva, L.R., Amitai, Y., and Connors, B.W. (1991). Intrinsic oscillations of neocortex generated by layer 5 pyramidal neurons. Science *251*, 432–435.

Steriade, M., McCormick, D.A., and Sejnowski, T.J. (1993). Thalamocortical oscillations in the sleeping and aroused brain. Science *262*, 679–685.

Traub, R.D., and Bibbig, A. (2000). A model of high-frequency ripples in the hippocampus based on synaptic coupling plus axon-axon gap junctions between pyramidal neurons. J. Neurosci. *20*, 2086–2093.

Turner, J.P., and Salt, T.E. (2000). Synaptic activation of the group I metabotropic glutamate receptor mGlu1 on the thalamocortical neurons of the rat dorsal lateral geniculate nucleus in vitro. Neuroscience *100*, 493–505.

Venance, L., Rozov, A., Blatow, M., Burnashev, N., Feldmeyer, D., and Monyer, H. (2000). Connexin expression in electrically coupled postnatal rat brain neurons. Proc. Natl. Acad. Sci. USA *97*, 10260–10265.

Whittington, M.A., Traub, R.D., and Jefferys, J.G. (1995). Synchronized oscillations in interneuron networks driven by metabotropic glutamate receptor activation. Nature *373*, 612–615.

Williams, S.R., and Stuart, G.J. (2000). Action potential backpropagation and somato-dendritic distribution of ion channels in thalamocortical neurons. J. Neurosci. *20*, 1307–1317.

Zhan, X.J., Cox, C.L., and Sherman, S.M. (2000). Dendritic depolarization efficiently attenuates low-threshold calcium spikes in thalamic relay cells. J. Neurosci. *20*, 3909–3914.

Zhu, J.J., Uhlrich, D.J., Xue, J.T., and Lytton, W.W. (1999). An intrinsic oscillation in interneurons of the rat lateral geniculate nucleus. J. Neurophysiol. *81*, 702–711.